Atomic Scale Insights into Flow-Accelerated Corrosion of SA106 Gr.B Carbon Steel in Simulated Secondary Water

Do Haeng Hur [a*], Jeoh Han [a]
[a] *Nuclear Materials Safety Research Division, Korea Atomic Energy Research Institute, Daejeon 34057*
[*] *Corresponding author: dhhur@kaeri.re.kr*

Keywords : flow-accelerated corrosion, SA106 Gr.B, oxide film, shear stress, point defect density

1. Introduction

Carbon steel piping in nuclear plants undergoes flow-accelerated corrosion (FAC). The key mechanism of FAC [1,2] is that the dissolution of an oxide layer at the water/oxide interface is accelerated with fluid velocity, while oxide is formed at the oxide/metal interface by the corrosion of the base metal, resulting in wall thinning of the piping. Therefore, it is deemed that there should be a lot of research on the characteristics of oxides, but atomic-scale characteristics of the oxide film remain still unknown. In addition, many studies state that oxide films formed under FAC conditions are porous without providing their own experimental evidence. These arguments originate from two studies: Castle and Mann [3] and Berge et al. [4]. However, their results were obtained in a static 13% NaOH solution, not in flowing water.

The differing nature of oxides formed during the corrosion damage of carbon steel in static and fast flowing water is crucial in that it can provide insights into how fluid flow plays a role in the formation and dissolution of oxide films. In this study, we systemically observed oxide films formed under static and dynamic water flow using scanning electron microscopy (SEM) and high-angle annular dark-field (HAADF) scanning transmission electron microscopy (STEM). The point defect concentrations in the oxide films were also estimated through a Mott-Schottky analysis.

2. Experimental Methods

2.1 Specimen Preparation

Specimens were manufactured by cutting SA106 Gr.B carbon steel using wire-cutting electrical discharge machining. The surfaces of the specimens were ground using SiC paper down to grit #1000, and then ultrasonically cleaned in acetone.

2.2 Corrosion Tests

A closed water circulation system was used for corrosion tests. The tests were conducted in simulated secondary water of a PWR: a solution with a $pH_{25°C}$ of 9.0. The pH of the solution was adjusted with ammonia and the level of dissolved oxygen was maintained below 2 μg/L by bubbling nitrogen gas.

Specimens were fixed in a regular dodecagonal-shaped specimen holder with Teflon bolts and nuts. The specimen holder was then attached to the drive shaft of a magnetic drive assembly that was installed on the lid of an autoclave. The solution entered the autoclave at a flow rate of 0.15 L/min at 20 bar by a high pressure pump, and the effluent solution was cooled and returned in a solution tank via pH and dissolved oxygen meters. The solution temperature adjacent to the specimens in the autoclave was maintained at 150 °C.

When these conditions were satisfied, two types of corrosion tests were performed separately. First, the specimen holder was rotated using the magnetic drive so that the water flow velocity at the surface of the specimens was 5 m/s. Second, a corrosion test was performed without rotating the magnetic drive. Therefore, the second test condition can be regarded as a static fluid condition (0 m/s). Each test duration was 500 h. When the test was over, the specimens was weighted using a balance with an accuracy of 10^{-5} g.

2.3 Oxide Characterization

The oxides formed on the specimens during the corrosion tests were observed using SEM. Cross-sectional foils for a transmission electron microscopy (TEM) analysis were prepared by milling the oxide films using the focused ion beam technique. The images and diffraction patterns of the films were examined using TEM at an acceleration voltage of 200 kV.

2.4 Electrochemical test

Capacitances measurements were performed to examine the charge carrier density of the oxide films formed during the corrosion tests under the two different water flow conditions. The capacitances measurements for the Mott-Schottky analysis were conducted in a borated buffer solution (0.05 M H_3BO_3 + 0.075 M $Na_2B_4O_7$) at ~23 ℃. A sinusoidal excitation with an amplitude of 10 mV was applied at a frequency of 1 kHz and a potential step rate of 20 mV in the cathodic potential direction from +1.0 V to –0.5 V vs. saturated calomel reference electrode (SCE).

3. Results and Discussion

The corrosion rate of SA106 Gr.B carbon steel was 0.44 μg/cm^{2}h under the static fluid condition. However, it was drastically accelerated approximately 12 times to 5.20 μg/cm^{2}h under the dynamic fluid condition of 5

m/s. This result, although expected, demonstrates why this phenomenon is designated as FAC.

As shown in Fig. 1, under the static condition, the surface was densely covered with polyhedral-shaped particles less than approximately 400 nm. A compact and thin oxide layer was observed on the cross-section of the specimens. However, under the turbulent condition, the oxide particles exhibited very irregular, crumb-like shapes without a defined or multi-faceted shape. Furthermore, the particles were so sloppy that microscopic voids were observed as marked by the yellow-dotted circles. The cross-section of the sample clearly showed that the oxide layer was very porous.

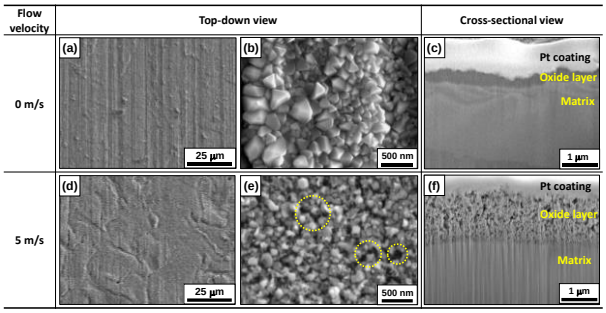

Fig. 1. SEM images of the surfaces and cross-sections of the oxides formed on SA106 Gr.B: (a, b, c) in static water, and (d, e, f) in turbulent water at a flow velocity of 5 m/s.

Fig. 2 shows the atomic resolution HAADF-STEM micrographs of the oxide films formed under the static and turbulent flow conditions. The lattice fringes of the static oxides were very distinct, highly ordered, and parallel (Fig. 2a), indicating that the oxide has very high crystallinity and the lattice planes have few crystal defects. Nevertheless, some localized spots with blurred lattice fringes were observed, as shown by the yellow arrows, indicating the existence of vacancy-type defects at the sites. However, in the dynamic oxides (Fig. 2b), the lattice fringes revealed much more obscure and discontinuous characteristics, as indicated by the arrow heads, although some blurred spots were observed. Slightly disordered regions were also observed, as indicated by the dotted circles. These all give rise to abundant defects around the sites.

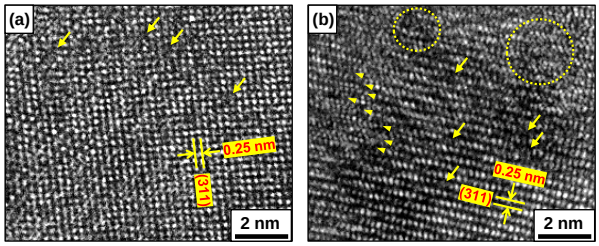

Fig. 2. HAADF-STEM images of the oxides: (a) in static water, and (b) in turbulent water at a flow velocity of 5 m/s.

As shown in in Fig. 3, the space charge capacitances of the dynamic oxide were approximately 4 times larger than those of the static oxide. This indicates that the resistance of the dynamic oxide is much larger than that of the static oxide. The charge charrier density was calculated using the Mott-Schottky relation [5] and slopes of the plots in Fig. 3. The total charge carrier density of the dynamic oxide film was approximately 7 times higher than that of the static oxide film. This result indicates that the dynamic oxide film is highly defective at the atomic scale, in agreement with the STEM images of Fig. 2. It is clear that charge transfer through the defective oxide film is facilitated, resulting in an increased corrosion rate.

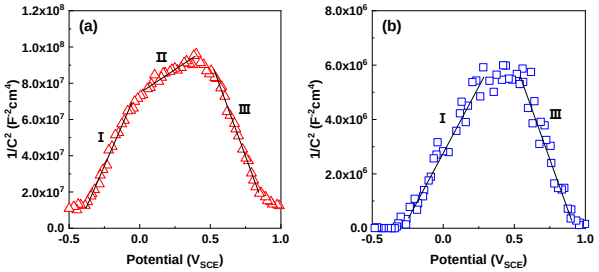

Fig. 3. Mott-Schottky plots of oxide films formed on SA106 Gr.B: (a) in static water, and (b) in turbulent water at a flow velocity of 5 m/s

Turbulence flow increases shear stress as well as mass transfer on the specimen surface. The calculated shear stress was 119 Pa under the test condition of this work at 150 °C and a flow velocity of 5 m/s.

In the process of magnetite formation, shear stress under a turbulent flow can distort the atomic arrangement. The mis-fitted aspects of the oxide lattice fringes observed in Fig 2b cannot be interpreted from the fast dissolution and mass transfer effect point of view. Therefore, the origin of these characteristics is attributed to the shear stress applied to the growing magnetite layers. In addition, attaching of the iron ions from the water to the outermost layer of the oxide is hindered by the shear stress, leading to miss-fits of the oxide lattice. Similarly, the escape of iron ions may be assisted by the hydrodynamic shear force.

Dissolution of iron ions from the magnetite lattice into the solution leaves metal cation vacancies in the lattice. As a result, oxygen vacancies are created in the oxide to maintain the condition of charge neutrality [6]. Eventually, as FAC progresses, the point defect density increases. Here, the cation vacancies act as electron acceptors and the oxygen vacancies as electron donors in the semiconducting oxide. Therefore, the Mott-Schottky tests clearly reveal a drastic increase in the atomic-scale defect density of the dynamic oxide, in agreement with the STEM image.

4. Conclusions

We have provided evidence for the correlation between the corrosion rates and the oxide properties of

carbon steel. Atomic-scale STEM observations demonstrate the existence of abundant lattice defects in the oxide film formed in fast turbulent water, which is attributed to hydrodynamic shear stress. A sharp increase of point defects is further confirmed by a Mott-Schottky analysis of the oxide film. These defects act as diffusion paths of anions and cations through the film, resulting in an increase of FAC rates. Our results provide new insights into the role of flow velocity in the formation and dissolution process of oxide films at the atomic scale.

Acknowledgements

This study was supported by the National Research Foundation (NRF) grant funded by the government of the Republic of Korea (RS-2022-00143316).

REFERENCES

[1] P. Khunphakdee, B. Chalermsinsuwan, Review of flow accelerated corrosion mechanism, numerical analysis, and control measures, Chemical Engineering Research and Design 197 (2023) 519–535.
[2] R.B Dooley, Flow-accelerated corrosion of fossil and combined cycle/HRSG plants, PowerPlant Chemistry 10 (2008) 68−89.
[3] J.E. Castle and G.M.W. Mann, The mechanism of formation of a porous oxide film on steel, Corrosion Science 6 (1966) 253–262.
[4] Ph. Berge, C. Ribon, P. Saint Paul, The effect of hydrogen on the corrosion of steels in high temperature water, Corrosion 32 (1976) 223–228.
[5] L.V. Taveira, M.F. Montemor, M. Da Cunha Belo, M.G. Ferreira, L.F.P. Dick, Influence of incorporated Mo and Nb on the Mott–Schottky behavior of anodic films formed on AISI 304L, Corrosion Science 52 (2010) 2813–2818.
[6] D.H. Hur, S.H. Jeon, J. Han, S.Y. Park, Y.B. Chun, Effect of gadolinium addition on the corrosion behavior and oxide properties of titanium in boric acid solution at 50 ℃, J. Materials Research and Technology, 21 (2022) 3051–3061.